

**ORBITAL DEBRIS AND METEOROID POPULATION  
AS ESTIMATED FROM LDEF IMPACT DATA**

Jingchang Zhang  
Lockheed Engineering & Sciences Company, 2400 NASA Road 1, C102,  
Houston, TX 77058  
Phone: (713) 333-6266, Fax: (713) 333-7791

Donald J. Kessler  
NASA Johnson Space Center, Houston, TX 77058  
Phone (713) 483-5313, Fax: (713) 483-5276

**SUMMARY**

Examination of LDEF's various surfaces shows numerous craters and holes due to hypervelocity impacts of meteoroids and man-made orbital debris. In this paper, the crater numbers as reported by Humes (Refs. 1 and 2) have been analysed in an effort to understand the orbital debris and natural meteoroid environment in LEO. To determine the fraction of man-made to natural impacts, the side to top ratio of impacts (Ref. 1) and results of the Chemistry of Micrometeoroids Experiment (CME, Refs. 3 and 4) are used. For craters in the 100  $\mu\text{m}$  to 500  $\mu\text{m}$  size range, about 25% to 30% of the impacts on the forward-facing surfaces and about 10% of the impacts on the trailing surfaces were estimated due to man-made orbital debris. A technique has been developed to convert crater numbers to particle fluxes, taking the fact into account that the distributions of impact velocity and incidence angle vary over the different surfaces of LDEF, as well as the ratio of the surface area flux to the cross-sectional area flux. Applying this technique, Humes's data concerning craters with limiting lip diameters of 100  $\mu\text{m}$ , 200  $\mu\text{m}$  and 500  $\mu\text{m}$  have been converted into orbital debris and meteoroid fluxes ranging from about 20  $\mu\text{m}$  to 200  $\mu\text{m}$  particle diameter. The results exhibit good agreement with orbital debris model (Kessler, et al., Ref. 5) and meteoroid model (Grun et al., Ref. 6). The converted meteoroid flux is slightly larger than Grun's model (by 40% to 70%). The converted orbital debris flux is slightly lower than Kessler's model for particle diameter smaller than about 30  $\mu\text{m}$  and slightly larger than the model for particle diameter larger than about 40  $\mu\text{m}$ . Taking also into account the IDE data point at about 0.8  $\mu\text{m}$  particle diameter, it suggests to change the slope  $\log(\text{flux})$  versus  $\log(\text{diameter})$  of orbital debris flux in the 1  $\mu\text{m}$  to 100  $\mu\text{m}$  particle diameter range from 2.5 (used in the model, Ref. 5) to 1.9.

**INTRODUCTION**

Since the Long Duration Exposure Facility (LDEF) was recovered in January 1990, many investigators have examined its 14 facing surfaces and analysed craters and holes caused by meteoroid and man-made debris impacts. Very recently, more data concerning craters from 100  $\mu\text{m}$  to 1000  $\mu\text{m}$  lip diameter were published (Ref. 1), and they can be evaluated to understand the particle environment of orbital debris and natural meteoroids.

The percentage of orbital debris versus meteoroids is of great importance to understanding the LDEF data. Chemical analysis of impact residues provides the possibility of distinguishing between them. However, little data on chemical analysis has been published so far. Pending the publication of more chemical results in the future, we will attempt to estimate the orbital debris fraction from the analysis of orbital dynamics and from other theoretical considerations.

LDEF was unique in that the spacecraft maintained a fixed orientation with respect to the Earth and the orbital velocity vector. This means that directional properties must be considered before comparing LDEF's measured flux with other experiments or models which are usually defined in terms of the flux on a randomly tumbling surface, or "randomly tumbling surface area" flux. It is also common to use the flux through a given cross-sectional area, or "cross-sectional area" flux which is 4 times the "randomly tumbling surface area" flux. Due to its fixed orientation, the flux measured on LDEF is in terms of the flux on an oriented surface, or "oriented surface area" flux. It becomes necessary to find the relation between the "oriented surface area" flux and the "cross-sectional area" flux which is a function of the surface orientation. In addition, one has also to find the relation between the crater diameter and the particle diameter which varies over the different surfaces also. A technique will be presented which can be utilized to conduct such a conversion properly. Using this technique, the data for craters to a limiting lip diameter of 100  $\mu\text{m}$ , 200  $\mu\text{m}$  and 500  $\mu\text{m}$  in Refs. 1 and 2 will be converted to orbital debris and meteoroid fluxes.

This technique was previously used in Ref. 7 to convert the 500  $\mu\text{m}$  data where 46% orbital debris on the forward-facing surface at 52° yaw and 15% orbital debris on the trailing surface at 172° yaw were assumed. However, according to the analysis in this paper, a lower fraction of orbital debris impacts seems to be more appropriate. The 500  $\mu\text{m}$  data will be therefore reanalysed in this paper and a slightly lower orbital debris flux and a slightly larger meteoroid flux than obtained in Ref. 7 is expected.

### LDEF IMPACT DATA AND ESTIMATION OF MAN-MADE DEBRIS FRACTION

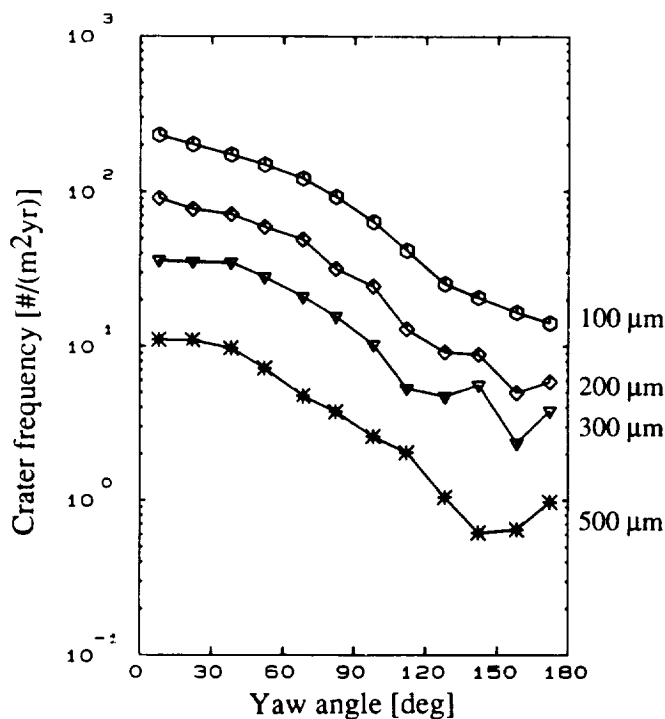
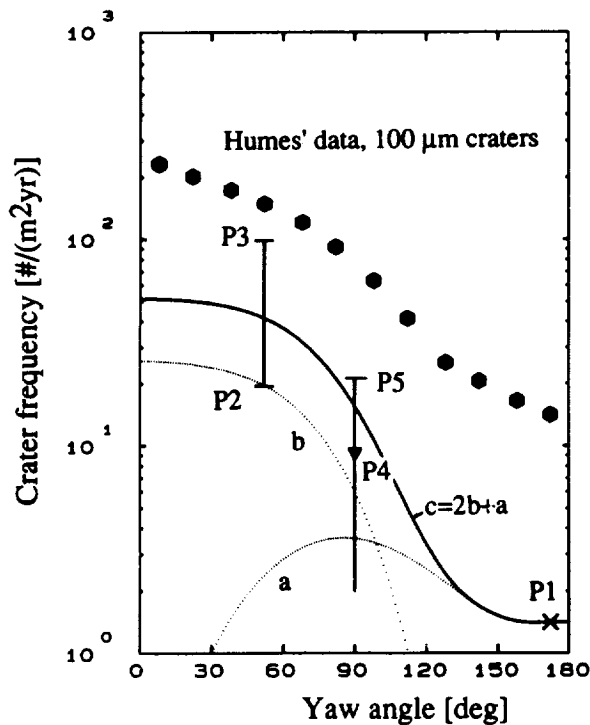


Fig. 1. LDEF impact data of Humes (Refs. 1 and 2).

Fig. 1 illustrates the LDEF impact data of Humes (Refs. 1, 2). Impact frequencies of craters with a limiting lip diameter of 500, 300, 200 and 100  $\mu\text{m}$  are given as a function of the yaw angle which is defined relative to the velocity vector of LDEF. With decreasing crater size, the crater numbers increase. This results in a reduction of statistical fluctuations with decreasing crater size. This is the reason why the curves for smaller craters are more in accordance with theoretical considerations (become smoother and decrease from LDEF's leading surface to trailing surface).

The data in Fig. 1 contain natural meteoroid impacts as well as man-made debris impacts. A major step in evaluating the particle population is to know the fraction of debris impacts versus meteoroid impacts. Chemical analysis of impact residues provides the possibility of distinguishing between them. The results of the Chemistry of Micrometeoroids Experiment (CME) (Refs. 3, 4) will be used for this purpose. However, the CME results do not give the percentage immediately because: i) They are only performed on two LDEF surfaces, namely one on the trailing surface (172° yaw) and another on a forward-facing surface at 52° yaw; ii) about 50% of the craters cannot be identified as man-made or natural since no residue is left or the residue contains the same material as the experiment plate.

Therefore, other considerations are required to estimate the fraction of man-made versus natural particles. In the following, these will be performed by considering only the  $>100 \mu\text{m}$  craters, illustrated in Fig. 2.



**Fig. 2. Estimation of the percentage of orbital debris versus meteoroids. Two particle orbits are used:  $a=400\text{km}\times 36000\text{km}/28.6^\circ$ ,  $b=400\text{km}\times 500\text{km}/100^\circ$ .**

determined to be meteoroid impacts, while 53% could not be identified. The lower density of aluminum (versus gold) means that for a given velocity, vaporization is less likely; however, debris velocities on the forward-facing surface are considerably higher than on the trailing surface, making vaporization of debris more probable than on the trailing surface. On the other hand, one must assume that a considerable fraction of the unknown craters is due to aluminum debris impacts which cannot be detected on aluminum surfaces, since about 80% of man-made impacts found on the gold plate contains only aluminum. However, it is hard to determine the exact percentage. At this point, one knows only that the debris fraction ranges somewhere between 13% (if all unknown craters would be assumed to be natural origin) and 67% (if all unknown craters would be assumed to be man-made origin). P2 and P3 in Fig. 2 indicate this range.

As an additional help, we can use the ratio of impacts on LDEF's side (at  $90^\circ$  yaw, which is the average of fluxes on the surfaces at  $82^\circ$  and  $98^\circ$  yaw) to impacts on the top. If there would be only meteoroid impacts, the only difference between the fluxes on the side and top is the Earth shielding effect which reduces the flux on the side. This flux ratio was calculated using meteoroid models and found to be about 0.71 for  $100 \mu\text{m}$  craters according to Ref. 8. Because there are debris impacts on the side, but almost no debris impacts on the top, the measured side to top ratio of all impacts is larger than that of meteoroid impacts alone. The difference between the measured side/top ratio and the modeled meteoroid side/top ratio enables us to determine the debris/meteoroid ratio on the side.

One of the CME collectors is the gold plate on LDEF's trailing surface. 15% of the impacts on the gold plate was determined to be man-made, 29% was determined to be natural while 56% had no residue so their source is unknown. Considering only craters  $> 100 \mu\text{m}$ , the debris fraction is 10% and meteoroid fraction is 32.5% while 57.5% is unknown. As discussed in Ref. 4, the major loss process of projectile residue on the gold plate is vaporization of the projectile. Since debris particles encounter the trailing surface only with low velocities, they are not likely to be vaporized. Therefore, all impacts with no residue will be assumed to be natural. As a result, 90% of craters  $> 100 \mu\text{m}$  is then determined to be natural and only 10% to be man-made. The 10% : 90% ratio of debris versus meteoroids on the trailing surface will be used in this paper. P1 in Fig. 2 indicates the 10% debris impacts point.

CME has also an aluminum plate located in Bay A11,  $52^\circ$  yaw. On the Al-plate, 13% of all craters  $> 100 \mu\text{m}$  was determined to be debris impacts (but non-aluminum, because aluminum debris cannot be identified on the Al-plate). 34% was

As reported in Ref. 1, the measured side/top ratio of 100  $\mu\text{m}$  craters amounts to 0.82 (the nominal ratio). If taking the upper limit of 90% confidence on the side and the lower limit of 90% confidence on the top, this ratio increases to 0.97 (the upper limit of 99% confidence). An additional uncertainty results from the lack of precise calibration between the top and side surfaces. According to Ref. 1, the top surface appeared to have different properties than the other surfaces. It was smoother and had a different color, indicating it was not cleaned and anodized like the other surfaces. As a result, the top surface might make a crater with a lip that would measure larger than an anodized surface. For example, a 10% increase in the crater diameter resulting from a given debris impact would result in about a 25% increase in flux. Therefore, a 10% crater diameter error would easily put the nominal value for the side to top ratio near the upper limit of 99% confidence limit.

The ratio of debris to all craters on the side can be determined as:

$$P_d = \frac{1 - r_m / r_{m+d}}{1 - r_m / r_d} \quad (1)$$

where

- $P_d$ : fraction of debris craters to all craters on the side;
- $r_d$ : side/top ratio of debris craters (large, since debris impacts on the top are negligible);
- $r_m$ : side/top ratio of meteoroid craters, can be calculated using meteoroid model;
- $r_{m+d}$ : side/top ratio of all craters, is measured on LDEF.

If debris impacts on the top are neglected, Eq. (1) becomes:

$$P_d = 1 - \frac{r_m}{r_{m+d}} \quad (2)$$

According to Ref. 8,  $r_m$  is 0.71, if the mean LDEF altitude is assumed to be 460 km, atmospheric height to be 150 km and the slope  $\log(\text{flux})$  versus  $\log(\text{mass})$  to be -0.48. The nominal debris fraction on the side is then 13% (P4 in Fig. 2) and the upper limit with 99% confidence is 27% (P5 in Fig. 2).

It should be noted that the calculated side/top ratio of meteoroid craters depends on the assumption of atmospheric height and the slope  $\log(\text{flux})$  versus  $\log(\text{mass})$ . In Ref. 1, this ratio is calculated in a different way, and  $r_m = 0.63$  is obtained. The debris fraction on the side would be thereafter 22% with an upper limit of 34%. Combined with the lack of precise calibration, the debris fraction might exceed 50%. In the following, however, the 13% fraction is still considered as the nominal fraction.

The question now becomes how to find a debris curve which best fits the data points at 52°, 90° and 172° yaw angles (P1 to P5). The debris point at 90° represents a strict constraint, since all debris orbits which produce a considerable flux either on the trailing surface (172° yaw) or on the forward-facing surface (52° yaw) also contribute a large flux on LDEF's side (Refs. 9, 10). There are not many possibilities which keep the flux at 90° yaw low. The best way to keep the flux on the side low is to use the following two particle orbits:

- a) Highly elliptical orbit with about 28.6 deg inclination (curve a in Fig. 2) to account for debris impacts on the trailing surface, and

- b) Near-circular orbit with about 100 deg inclination (curve b in Fig. 2) to account for debris impacts on the forward-facing surface. The logic for 100° inclination will be discussed later and is demonstrated in Figure 3.

Curve a in Fig. 2 is normalized to pass through P1 and curve b is normalized to pass through P2. With curve b, only non-aluminum debris impacts on the forward-facing surface are simulated. As reported in Ref. 4, the ratio of aluminum debris to non-aluminum debris on the trailing surface is about 5:1. This suggests one has to assume more aluminum debris impacts than non-aluminum debris impacts on the Al-plate. But one cannot assume too many aluminum debris impacts, because it would lead to a debris flux on the side exceeding the upper limit (P5). The best fit results from assuming as many aluminum debris impacts originating from the 100 deg orbit as the measured 13% of non-aluminum debris impacts. This results in a total of 28% debris impacts on the Al-plate (26% from the 100 deg orbit, 2% from the 28.6 deg orbit). The total debris curve (curve c in Fig. 2) is then obtained by multiplying curve b by 2 and adding to curve a. The debris fraction on the side (90° yaw) is thereafter 20%. These percentages are summarized in Table 1.

Table 1. Estimated Fraction of Debris Craters on the Forward-Facing Surface (52° Yaw), the Side (90° Yaw) and the Trailing Surface (172° Yaw)

52 deg	90 deg	172 deg
28%	20%	10%

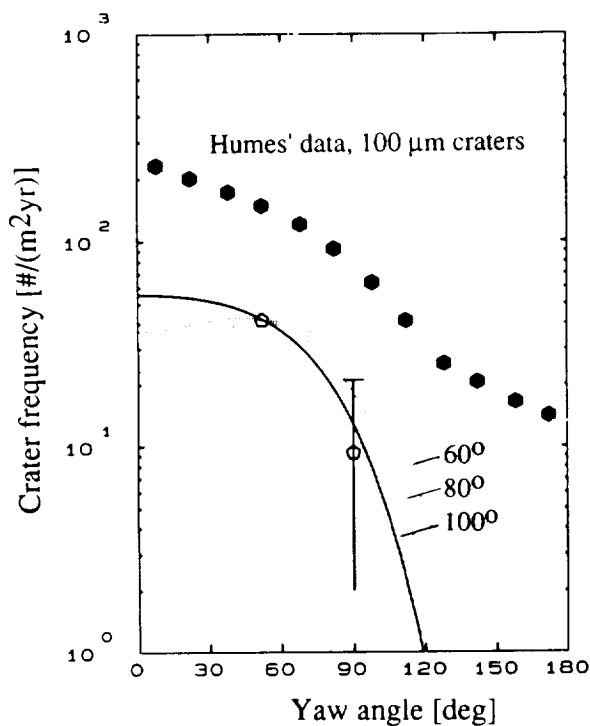


**Fig. 3. Crater distribution which would be produced on LDEF from particles in near-circular orbits with various inclinations. Curves are normalized to pass through the measurement point at 52° yaw angle.**

The orbital parameter model using the two debris particle orbits mentioned above will be called the "Two-Particle-Orbits-Model" in the following. The reason why 100 deg inclination, not other inclinations like 60 deg or 80 deg, is being considered as the best fit is shown in Fig. 3. All three curves are normalized to pass through the 28% debris point at 52 deg yaw. Only the 100 deg inclination keeps the flux on the side (90 deg yaw) close to the nominal debris point (P4), while other inclinations produce a flux on the side which is too high. The 60 deg curve even exceeds the upper limit with 99% confidence (P5). For the same reason, the 28.6 deg inclination orbit is considered as the best choice to account for debris impacts on the trailing surface.

The use of only two orbits to represent the orbital debris population is not to say that the population consists of only these orbits; rather these two orbits approximate the actual distribution of orbits. The fact that the direction and velocity distribution resulting from these two orbits matches (within the uncertainty of measurements) that using the "modified catalogue" distribution in Ref. 9 is a justification for this use. The Two-Particle-Orbits-Model is

aimed to convert the crater diameter to particle diameter and to convert the oriented surface area flux to cross-sectional area flux, and it appears to perform such a conversion properly.

The man-made debris fraction for 100 μm craters estimated above will also be assumed to apply for craters as large as 500 μm. This seems to be valid as the side to top ratios of Humes's data (Ref. 1) do not show significant variation from 100 μm to 500 μm.

The debris and meteoroid impacts determined for 100 μm, 200 μm and 500 μm craters using above debris/meteoroid percentages are summarized in Table 2. It should be noted that the sum of debris impacts plus meteoroid impacts in Table 2 varies slightly from Humes's data. The modeled values are smoother than the measurement and are considered as the actual fluxes after removing statistical fluctuations.

Table 2. Estimated Debris and Meteoroid Impacts for 100 μm, 200 μm and 500 μm Craters from Humes's Data (Refs. 1 and 2)

yaw angle [deg]	100 μm craters [#m <sup>-2</sup> yr]		200 μm craters [#m <sup>-2</sup> yr]		500 μm craters [#m <sup>-2</sup> yr]	
	debris	met.	debris	met.	debris	met.
8	55.7	159.5	20.5	65.6	2.52	8.97
22	52.9	151.2	20.0	61.7	2.45	8.40
38	47.9	132.9	18.7	54.1	2.30	7.28
52	41.5	112.0	16.4	44.4	2.02	5.88
68	33.7	86.5	12.8	34.2	1.57	4.44
82	23.7	65.7	8.25	24.9	1.02	3.17
98	13.5	46.2	4.27	17.5	0.527	2.17
112	5.81	33.2	1.83	11.9	0.227	1.45
128	2.39	22.7	0.869	8.16	0.108	0.974
142	1.52	17.0	0.577	5.89	0.0721	0.697
158	1.43	13.4	0.488	4.68	0.0610	0.553
172	1.41	12.3	0.480	4.21	0.0600	0.497

### CONVERSION OF CRATER FREQUENCIES TO PARTICLE FLUXES

The conversion of the LDEF impact data to particle flux will be accomplished in two steps:

- a) Conversion of the crater diameter to particle diameter,
- b) Conversion of the crater numbers to cross-sectional area flux.

For the first step, relation between particle size and crater size is needed. It is very common to use the following hypervelocity impact equation (Ref. 2) which is based on laboratory tests:

$$t_{\infty} = C_1 \rho^{0.519} d^{1.056} (v \cos \theta)^{2/3} \quad (3)$$

where  $t_{\infty}$ =crater depth,  $\rho$ =density of the particle,  $d$ =particle diameter,  $v$ =impact velocity, and  $\theta$ =incidence angle measured from the normal to the surface; for aluminum plates,  $C_1=0.334$  for  $\rho$  in g/cm<sup>3</sup>,  $d$  in cm and  $v$  in km/s.

While Eq. (3) describes the crater depth, a relation to describe the crater diameter is needed, since the data in Refs. 1 and 2 are given to limiting crater lip diameters. As reported in Ref. 2, the lip diameter of most craters observed on LDEF is about 8/3 times the crater depth. Thus, the crater diameter can be expressed as:

$$D_r = C_2 \rho^{0.519} d^{1.056} (v \cos \theta)^{2/3} \quad (4)$$

where  $D_r$ =crater lip diameter; for aluminum plates,  $C_2=0.891$  for  $\rho$  in  $\text{g/cm}^3$ ,  $d$  in cm and  $v$  in km/s.

Since the impact velocity and the incidence angle are not measured on LDEF, Eq. (4) cannot directly be used to obtain the particle diameter from the crater diameter. As a common technique, averaged impact velocities and incidence angles are used. We denote the average velocity of the impacts as  $v_a$  and the average angle of the impacts as  $\theta_a$ , both referring to a limiting crater diameter and denoting the average diameter of particles which produce the crater diameter of  $D_r$  as  $d_a$ .

The quantities of  $v_a$  and  $\theta_a$  can be determined by applying the technique in Ref. 11 for transformation of a flux to a limiting particle size into a flux to a limiting penetration thickness. On the assumption that the cumulative flux of particle diameter  $\geq d$  is proportional to  $d^{-p}$ , combined with Eq. (4), the following relation is obtained:

$$v_a \cos \theta_a = \left\{ \frac{\int_{v=0}^{\infty} \int_{\theta=0}^{\pi/2} n_{v,\theta}(v, \theta) (v \cos \theta)^{\frac{2/3p}{1.056}} d\theta dv}{\int_{v=0}^{\infty} \int_{\theta=0}^{\pi/2} n_{v,\theta}(v, \theta) d\theta dv} \right\}^{\frac{1.056}{2/3p}} \quad (5)$$

where  $n_{v,\theta}$  is the distribution of the impact velocity and incidence angle, referring to a limiting particle diameter;  $p$  is the slope  $\log(\text{flux})$  versus  $\log(\text{diameter})$  in the form  $F \sim d^{-p}$ .

Eq. (5) considers the fact that smaller particles with larger  $v \cos \theta$  can produce the same crater as larger particles with smaller  $v \cos \theta$ , and the number of particles increases with  $d^{-p}$  while the particle diameter decreases.

In order to formulate a general relation describing the ratio of average particle diameter to crater diameter, we introduce a  $q$ -factor as:

$$q = \frac{d_a^{1.056} \rho^{0.519}}{D_r} = \frac{1}{C_2} (v_a \cos \theta_a)^{-2/3} \quad (6)$$

Combining Eqs. (5) and (6) results in:

$$q = C_3 \left\{ \frac{\int_{v=0}^{\infty} \int_{\theta=0}^{\pi/2} n_{v,\theta}(v, \theta) (v \cos \theta)^{\frac{2/3 \rho}{1.056}} d\theta dv}{\int_{v=0}^{\infty} \int_{\theta=0}^{\pi/2} n_{v,\theta}(v, \theta) d\theta dv} \right\}^{\frac{-1.056}{\rho}} \quad (7)$$

where for aluminum plates  $C_3=1.122$  for  $\rho$  in  $\text{g/cm}^3$ ,  $d$  in  $\text{cm}$  and  $v$  in  $\text{km/s}$ .

After calculation of the factor  $q$  using Eq. (7), the averaged particle diameter  $d_a$  which produces the crater diameter  $D_r$  can immediately be obtained. For  $100 \mu\text{m}$ ,  $200 \mu\text{m}$ ,  $500 \mu\text{m}$  and  $1000 \mu\text{m}$  crater diameters, the results are illustrated in Fig. 4.

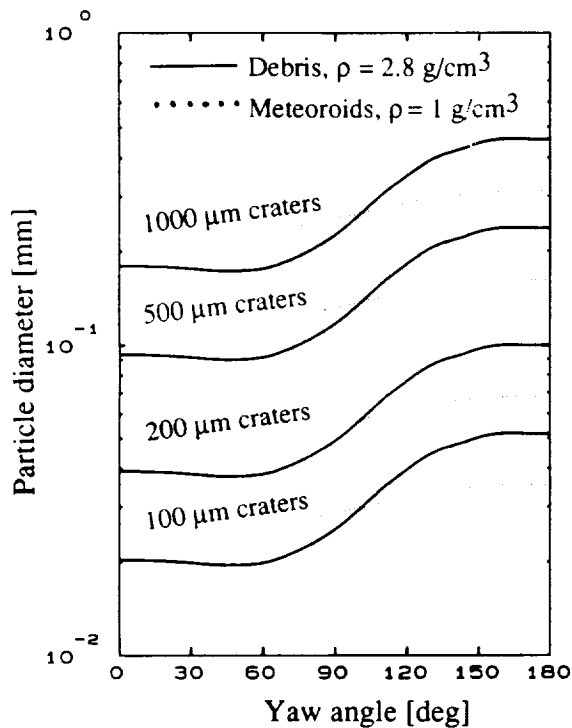


**Fig. 4. Average diameter of orbital debris and meteoroid particles producing craters with given crater lip diameters as indicated in the diagram.**

encountering the trailing surface with much lower velocities than encountering the leading surface. As a result, crater numbers of one crater size give more than one particle flux point. In other words, assuming a given crater diameter, each surface gives one particle size flux point.

The crater numbers measured on LDEF's various surfaces represent a flux on a flat plate with fixed orientation. This flux is to be converted to the cross-sectional area flux (flux on a unit sphere with  $1 \text{ m}^2$  cross-sectional area). If the surface area flux is obtained on a tumbling flat plate (like Solar Max), the cross-sectional area flux is 4 times the surface area flux. Considering surfaces with fixed orientation (like LDEF), the ratio of surface area flux to cross-sectional area flux depends on the surface orientation.

To obtain the results in Fig. 4, the distribution of velocity and incidence angle of debris impacts as well as meteoroid impacts for each surface of LDEF is needed. This distribution for debris impacts is obtained by applying the Two-Particle-Orbits-Model mentioned above, while that for meteoroid impacts is obtained by means of the same meteoroid model as used in Refs.7 and 10.

Fig.4 shows that a slightly larger meteoroid particle than debris particle is required to produce the same crater on LDEF's leading surface (about 1.2:1); this is due to the lower density of meteoroid particles. But to produce the same crater on the trailing surface, a larger debris particle than meteoroid particle is required (about 1.5:1), due to very low velocities of debris particles encountering the trailing surface. The particles producing a  $1000 \mu\text{m}$  crater is not exactly 10 times as large as particles producing a  $100 \mu\text{m}$  crater, as the particle diameter goes into the impact equation (4) with the power of 1.056.

The particle diameter that corresponds to a given crater diameter depends on which surface is considered. Fig. 4 shows that a debris particle producing a given crater size on LDEF's trailing surface needs to be about 2.5 times as large as a debris particle producing the same crater size on the leading surface, because of debris particles

Fig.5 illustrates the ratio of the oriented surface area flux to the cross-sectional area flux as a function of the yaw angle by applying the meteoroid and debris models. The two debris curves are obtained by means of the Two-Particle-Orbits-Model applied for 100  $\mu\text{m}$  craters, one by assuming the slope of  $\log(\text{flux})$  versus  $\log(\text{diameter})$  to be 1.5 and the other by assuming the slope to be 2.5. It should be noted that the ratio of the oriented surface area flux to the cross-sectional area flux for debris impacts is sensitive to the assumption of the slope. A different slope leads to a different fraction of particles on the two particle orbits to fit the measurement which results in a different ratio of surface area flux to cross-sectional area flux.

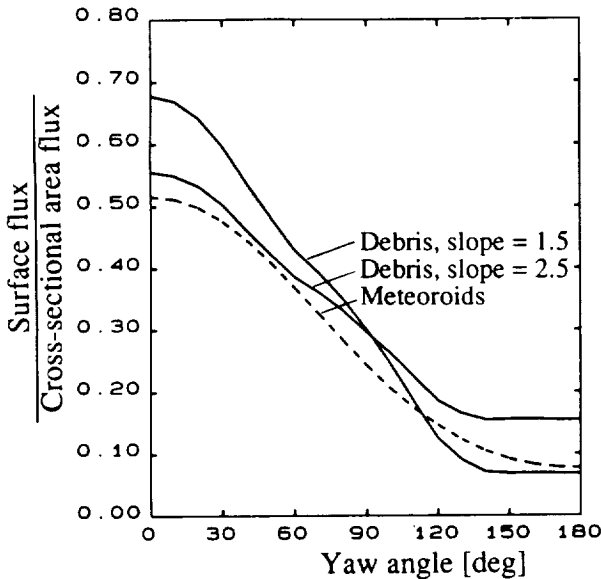


**Fig. 5. Ratio of surface flux to cross-sectional area flux. The ratios for orbital debris only apply for using the same assumptions as explained in the text.**

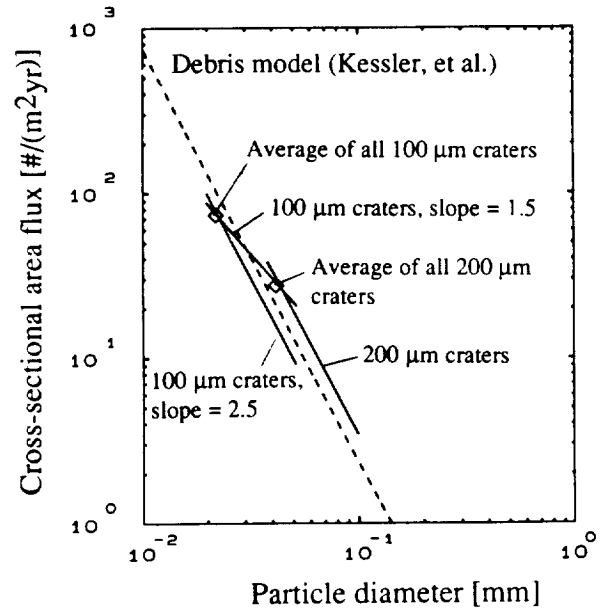


**Fig. 6. Conversion of craters > 100  $\mu\text{m}$  to orbital debris fluxes by assuming two different slopes of  $\log(\text{flux})$  versus  $\log(\text{diameter})$ .**

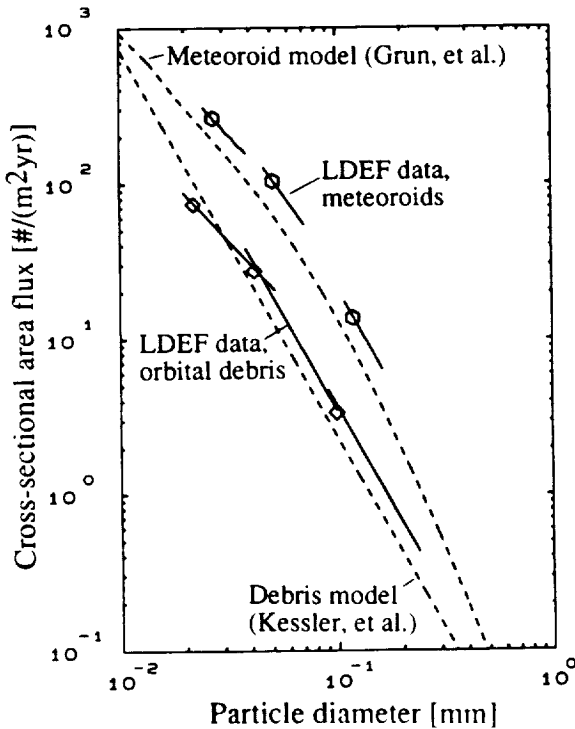
Fig. 6 shows the converted debris particle flux from 100  $\mu\text{m}$  debris craters for two assumptions of the slope  $\log(\text{flux})$  versus  $\log(\text{diameter})$ . The converted flux curves reflect exactly the slope assumed at the beginning, indicating no conceptual or mathematical errors were introduced.

The diamond symbols indicate an average flux of impacts on all 12 surfaces on LDEF's barrel. The particle diameter is obtained when the converted particle diameters on all 12 surfaces are averaged by weighting the flux on each surface. The flux is obtained when assuming all debris impacts are parallel to the Earth surface (which is valid if considering a spacecraft moving in low earth orbit). Under this assumption, the cross-sectional area flux is  $\pi$  times the flux on LDEF's barrel. Debris flux obtained in this way is not sensitive to various assumptions. With respect to the flux point obtained from 200  $\mu\text{m}$  craters, the 1.5 slope for 100  $\mu\text{m}$  craters can be considered a good choice.

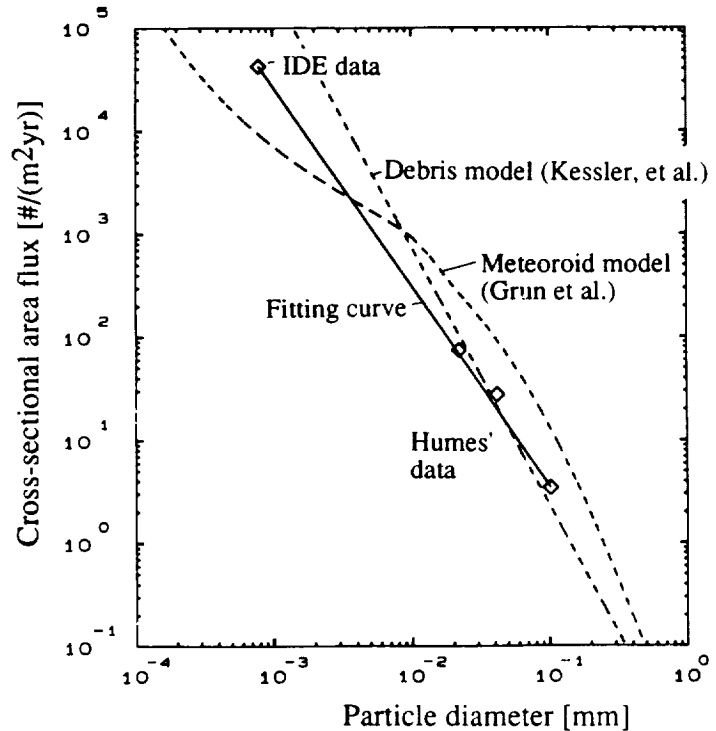
## RESULTS

Fig. 7 illustrates the debris and meteoroid fluxes converted from 100  $\mu\text{m}$ , 200  $\mu\text{m}$  and 500  $\mu\text{m}$  craters which cover a particle size range from 20  $\mu\text{m}$  to 240  $\mu\text{m}$  for man-made orbital debris and from 25  $\mu\text{m}$  to 160  $\mu\text{m}$  for meteoroids.

The debris fluxes are obtained by means of two different slopes. While the 100  $\mu\text{m}$  craters are converted using a slope of 1.5, a slope of 2.5 is used for 200  $\mu\text{m}$  and 500  $\mu\text{m}$  craters. The meteoroid fluxes are obtained by means of three different slopes: for 100  $\mu\text{m}$  craters using a slope of 1.5, for 200  $\mu\text{m}$  craters using a slope of 2 and for 500  $\mu\text{m}$  craters using a slope of 2.5.



**Fig. 7. Orbital debris and meteoroid fluxes converted from Humes's data for craters > 100  $\mu\text{m}$ , 200  $\mu\text{m}$  and 500  $\mu\text{m}$ .**



**Fig. 8. Orbital debris flux converted from Humes's data and IDE data compared to orbital debris model.**

The symbols (hexagon symbols for meteoroids and diamond symbols for orbital debris) represent an average flux of debris or meteoroid fluxes on all 12 surfaces around LDEF. To obtain the average debris flux, the cross-sectional area flux is assumed to be  $\pi$  times the surface area flux around LDEF, as explained in Fig. 6. To obtain the average meteoroid flux, the cross-sectional area flux is assumed to be 3.8 times the surface area flux around LDEF, since according to our meteoroid model, the ratio of the meteoroid flux on LDEF with fixed orientation to that on a tumbling LDEF (hypothetical) is 4:3.8.

A comparison to the debris model in Ref. 5 shows a good agreement. For particle diameter larger than 40  $\mu\text{m}$ , the measurement is slightly larger than the model, while for particle diameter smaller than 30  $\mu\text{m}$ , the measurement is slightly lower than the model. There is also a good agreement between converted meteoroid flux and the meteoroid model in Ref. 6. In general, the measured flux is slightly larger (by 40% to 70%) than the flux from the model.

In Ref. 12, fluxes to a limiting crater diameter of 3  $\mu\text{m}$  measured on six surfaces from the Interplanetary Dust Experiment (IDE) are reported. These fluxes result in an averaged cross-sectional area flux of 4.2  $\#/(m^2\text{yr})$  at 0.79  $\mu\text{m}$  particle diameter. Because the IDE measured mainly orbital debris swarms (Ref. 12), the fraction of meteoroid impacts can be neglected, and the flux of 4.2  $\#/(m^2\text{yr})$  will be considered

only due to orbital debris impacts. The IDE data point and the three orbital debris flux points from Humes's data are compiled in Fig. 8. It suggests using a  $\log(\text{flux})/\log(\text{diameter})$  slope of 1.9 to fit all of the four data points, as the solid line indicates. It differs from the model in Ref.5 where a slope of 2.5 is used. At 1  $\mu\text{m}$  particle diameter, the measurement is lower than the model by about one order of magnitude.

## CONCLUSIONS

The fraction of orbital debris impacts versus meteoroid impacts was analysed for craters in the 100  $\mu\text{m}$  to 500  $\mu\text{m}$  size range. The results indicate a slightly smaller debris population than previous analysis due to better statistics and applying more constraints. The best estimate of the debris population is 28% at 52° yaw and 10% on the trailing surface. However, there is still sufficient uncertainty that the previous results (of 46% & 15%, respectively) are possible. This has to be verified in the future when more chemical data are available.

Humes's data concerning craters from 100  $\mu\text{m}$  to 500  $\mu\text{m}$  in lip diameter were converted to orbital debris and meteoroid fluxes, ranging from 20  $\mu\text{m}$  to 240  $\mu\text{m}$  particle diameter for man-made orbital debris and from 25  $\mu\text{m}$  to 160  $\mu\text{m}$  particle diameter for meteoroids. At larger particle size range, the measured debris flux is slightly larger than the debris model (Kessler et al., Ref. 5), while the measured debris flux is lower than the model at smaller size range. The measured meteoroid flux is 40% to 70% larger than the meteoroid model (Grun et al., Ref. 6). However, if the debris population were about a factor of 2 higher, the meteoroid flux measured by LDEF would be very close to the meteoroid model.

The major uncertainties in the converted fluxes may result from two sources: i) How accurate is Eq. (3) used to convert the crater diameter to particle diameter; ii) How accurate is the estimated percentage of orbital debris versus meteoroids. The impact equation (3) was also used to convert previous impact data (e.g. Solar Max) on which the debris and meteoroid models are based. Therefore, the fluxes converted in this paper should be comparable to existing models. The uncertainty in the percentage of orbital debris versus meteoroids can be reduced when more chemical analyses of impact residues will be performed in the future.

Taking into account the IDE data which gave a debris flux at about 0.8  $\mu\text{m}$  particle diameter, the debris model in Ref. 5 is larger than the measurement at 1  $\mu\text{m}$  particle diameter by about one order of magnitude. The measurement suggests to reduce the  $\log(\text{flux})/\log(\text{diameter})$  slope from 2.5 to 1.9 in the 1  $\mu\text{m}$  to 100  $\mu\text{m}$  particle diameter range.

## ACKNOWLEDGMENT

We wish to thank Robert C. Reynolds for helpful discussions and constructive reviews of this manuscript. Significant suggestions were received from the referee Donald H. Humes which were gratefully incorporated into the paper.

## REFERENCES

1. Humes, D.H., "Small Craters on the Meteoroid and Space Debris Impact Experiment", Proc. of the 3rd LDEF Post-Retrieval Symposium, NASA CP-3275, 1995
2. Humes, D.H., "Large Craters on the Meteoroid and Space Debris Impact Experiment", Proc. of the 1st LDEF Post-Retrieval Symposium, NASA CP-3134, 1991, pp.399-418
3. Horz, F.; Bernhard, R.P., "Compositional Analysis and Classification of Projectile Residues in LDEF Impact Craters", NASA TM 104750, June 1992
4. Bernhard, R.P.; See, T.H.; Horz, F., "Projectile Compositions and Modal Frequencies on the 'Chemistry of Micrometeoroids' LDEF Experiment", Proc. of the 2nd LDEF Post-Retrieval Symposium, NASA CP-3194, 1993, pp.551-573
5. Kessler, D.J.; Reynolds, R.C.; Anz-Meador, P.D., "Orbital Debris Environment for Spacecraft Designed to Operate in Low Earth Orbit", NASA TM 100471, April 1989
6. Grun, E.; Zook, H.A.; Fechtig, H.; Giese, R.H., "Collisional Ballance of the Meteoritic Complex", Icarus 62, 1985, pp.244-272
7. Zhang, J.; Rex, D., "Decoding of the Particle Population from LDEF Crater Distributions", IAA.6.4-93-749, 44th I.A.F. Congress, Graz, Austria, Oct. 16-22, 1993
8. Zook, H.A., "Deriving the Velocity Distribution of Meteoroids from the Measured Meteoroid Impact Directionality on the Various LDEF Surfaces", Proc. of the 1st LDEF Post-Retrieval Symposium, NASA CP-3134, 1991, pp.569-579
9. Kessler, D.J., "Origin of Orbital Debris Impacts on LDEF's Trailing Surfaces", Proc. of the 2nd LDEF Post-Retrieval Symposium, NASA CP-3194, 1993, pp.585-593
10. Zhang, J.; Kessler, D.J.; Rex, D., "Interpretation of the Distribution of Large Craters on the Long Duration Exposure Facility (LDEF)", Proc. of the First European Conference on Space Debris, ESA SD-01, Darmstadt, Germany, 1993, pp.195-200
11. Kessler, D.J., "A Guide to Using Meteoroid-Environment Models for Experiment and Spacecraft Design Applications", NASA TN D-6596, March 1972
12. Simon, C.G., et al., "Long-Term Microparticle Flux Variability Indicated by Comparison of Interplanetary Dust Experiment (IDE) Timed Impacts for LDEF's First Year in Orbit with Impact Data for the Entire 5.77-Year Orbital Lifetime", Proc. of the 2nd LDEF Post-Retrieval Symposium, NASA CP-3194, 1993, pp.693-703